

## Counterion effects on the alkali dissolution mechanism of quartz

Yu-yun Yao<sup>1,3</sup>, Yun Tang<sup>1,2</sup>, Yong Yang<sup>1,2</sup>, Guo-hui Li<sup>1</sup>, Bo Wu<sup>1</sup>, Wen-zhi Dai<sup>1,2</sup>

<sup>1</sup> College of Mining, Guizhou University, Guiyang, China

<sup>2</sup> Guizhou Key Laboratory of Comprehensive Utilization of Nonmetallic Mineral Resources, Guiyang, China

<sup>3</sup> Mining Engineering and Geology College, Xinjiang Institute of Engineering, Urumqi, China

Corresponding authors: caseyty@163.com (Y. Tang), yyttmm1021@163.com (Y. Yong)

**Abstract:** In gold ore, quartz plays an important role in mineral formation by acting as the follower. Understanding counterion release, transport, and deposition in alkali solution is a prerequisite for evaluating the potential role of gold separate from quartz deposits in pretreatment. In this work, the aggregation, retention, and release of counterion in alkali solution media were investigated by kinetic research and pure mineral experiments, the correlation and mechanism of these processes were revealed by combining geochemical theory, interaction energy calculation, and quantum chemistry. The results showed that the retention and release of counterion were closely related to the dissolution and corrosion rate of quartz. The  $\text{NH}_4^+$  and  $\text{Fe}^{2+}$  with higher mineral affinity reduced the quartz stability, and the dispersion stability and mobility of the quartz were greatly improved by an alkaline substance due to the enhancement of steric hindrance effects. Quantum chemical calculation results show that ammonium ion promotes the dissolution of quartz stronger than ferrous ion, which is mainly reflected in reducing the activation energy required for the formation of transition state (TS1), which can be verified by kinetic calculation. These findings provide essential insight into the extraction of gold coated by quartz as well as a vital reference for the experiment of gold-loaded quartz leaching in mineral processing.

**Keywords:** quartz, counterion, quantum chemistry, hydrolysis, mechanism

### 1. Introduction

Undoubtedly, gold is an important strategic resource (Liu et al., 2019; Li et al., 2022; S. Zhang et al., 2021), but many golds are wrapped by quartz minerals and can't be recycled directly (Chen et al., 2019; Jian et al., 2021; Hunter et al., 2021). Therefore, in order to recover the coated gold, pretreatment is required before leaching (Gui et al., 2021). After pre-treatment, the gold-loaded quartz will be loose and porous, exposing the metallographic phase of the package, so that the gold can be perfectly complexed with the leaching agent, and the leaching rate of the gold can be improved. In a system of mixed reagents with non-ideal mixing effects in their slurry, various counterionic properties exhibit synergism or inhibitory interaction of dissolution and corrosion rate of quartz (DCRQ). The understanding of the interactions between quartz and slurry in the pre-treatment process is the key to taking advantage of counterion effects.

In comparison with the amount of work done on the influence of ions on the DCRQ in mineral water or an aqueous solution containing only one agent, the study of quartz in a slurry with complex agents is a rather limited field. Changing the alkaline cation of solutions provides the opportunity to study the role of pH, hydration radius, and hydrolysis constant effect on the DCRQ (A. Ali et al., 2017). Based on this study, it was found that in different solutions, the DCRQ in the order of  $\text{Ca}^{2+} < \text{Na}^+ < \text{K}^+$ , that is the synergism interaction in the KCl solution is even stronger. (Tamada et al., 2012) found that the presence of  $\text{Na}^+$  inhibited the formation of silicon atom five ligands in silica dissolution kinetics, resulting in the extension of Si-O distance and the weakening of bonding interaction, thus accelerating the fracture of the Si-O bond. (Al-Saedi et al., 2019) and other experimental simulations show that both quartz surface and carboxylate are negatively charged, and carboxylate will be repelled on the quartz surface unless it

is a positively charged  $-\text{COOCa}^+$  group that can bridge with the quartz surface. Lipatieva et al. (2022) and Cao et al. (2018) concluded that KOH solution is often used for highly selective etching of quartz and quartz etching in ternary solutions composed of  $\text{NH}_4\text{HF}_2$  + isopropyl alcohol + acetic acid has been investigated (Z. Zhang et al., 2017). The DFT calculations and experimental data clearly show that exposure to NaOH affects the structure and reactivity of quartz (A. M. Ali et al., 2020).

In the present work, for the first time, to our best knowledge, the influence of counterions produced by the pre-treatment of golden iron ore on quartz dissolution during the pre-treatment process of Carlin-type gold ore is being reported. Our team has been studying Carlin type gold ores (Ma et al., 2020; Tang et al., 2021), the main gold carrying minerals of this ore are pyrite and quartz. Both pyrite and the reagent initiator nano iron powder in the leaching process will produce  $\text{Fe}^{2+}$ . In addition, adding ammonium sulfate will introduce  $\text{NH}_4^+$ . Counterion effects of  $\text{Fe}^{2+}$  and  $\text{NH}_4^+$  has been studied. This paper reveals the dissolution behavior of quartz through pure quartz mineral experiments and uses quantum chemical calculations to explore the reaction mechanism of the quartz solution interface. It is well known that NaOH will react with quartz, but after the introduction of counterions ( $\text{NH}_4^+$  and  $\text{Fe}^{2+}$ ), the reaction needs to be studied. Here, the effect of counterions on the dissolution of alkali-leached quartz has been studied comprehensively using UV-VIS spectrophotometer, laser particle size analyzer, X-ray diffraction (XRD), scanning electron microscope (SEM) and energy dispersive spectrometer (EDS) techniques. A combination of techniques provides important information for exploring the mechanism of counterion. The research results provide a basis for the effective recovery of gold in gold-bearing quartz in Carlin-type gold mines.

## 2. Materials and methods

### 2.1. Materials

Pure quartz mineral was purchased from Chengdu Jinshan Chemical Reagent Co., Ltd. with a purity of 99.99%. After grinding and screening, take the particle size of +0.045 mm -0.074 mm and put it in the mineral sample bottle for sealing and storage. The relevant reagents used in the experiment are shown in Table 1.

Table 1 Experimental Reagents

Reagent name	Molecular formula	Purity	Manufacturer
Sodium hydroxide	NaOH	Analytically pure	Chengdu Jinshan Chemical Reagent Co., Ltd
Ammonium persulfate	$(\text{NH}_4)_2\text{S}_2\text{O}_8$	Analytically pure	Tianjin Kemio Chemical Reagent Co., Ltd
Ferrous sulfate heptahydrate	$\text{FeSO}_4 \cdot 7\text{H}_2\text{O}$	Analytically pure	Chengdu Jinshan Chemical Reagent Co., Ltd
Silicon standard solution	$\text{Na}_2\text{SiO}_3$	Analytically pure	Nonferrous Metals and Electronic Materials Analysis and Testing Center
Ammonium molybdate	$(\text{NH}_4)_2\text{MoO}_4$	Analytically pure	Tianjin No.4 Chemical Reagent Factory
Oxalic acid	$\text{H}_2\text{C}_2\text{O}_4$	Analytically pure	Tianjin Yongda Chemical Reagent Co., Ltd

### 2.2. Experimental method

The quartz dissolution test is carried out in a magnetic stirrer, and the reaction model is shown in Fig. 1. Add a certain concentration of alkaline substances into the reaction vessel, turn on the magnetic stirrer, and add 3 g of quartz ore sample and start timing. Take samples every 1 h, 5 mL each time, filter and dilute the leaching solution samples immediately, use the silicate ion concentration in the solution to reflect the dissolution of quartz, and analyze the silicate ion concentration in the solution was with a UV-VIS spectrophotometer. For example, take 3 g of +0.045 mm-0.074 mm sample respectively and put

it into a 500 mL polytetrafluoroethylene beaker, in which 1# 300 mL solution is prepared according to 3 mol/L NaOH concentration, 2# 300 mL solution is prepared according to 3 mol/L NaOH concentration and 0.02 mol/L  $\text{NH}_4^+$  concentration and added into the beaker, 3# 300 mL solution is prepared according to 3 mol/L NaOH concentration and 0.05 mol/L  $\text{Fe}^{2+}$  concentration and added into the beaker. Carry out the experiment at room temperature and take samples every 1 h, 5 mL of samples are taken each time for analysis. After the dissolution test, the leaching residue shall be filtered and dried, and then stored.

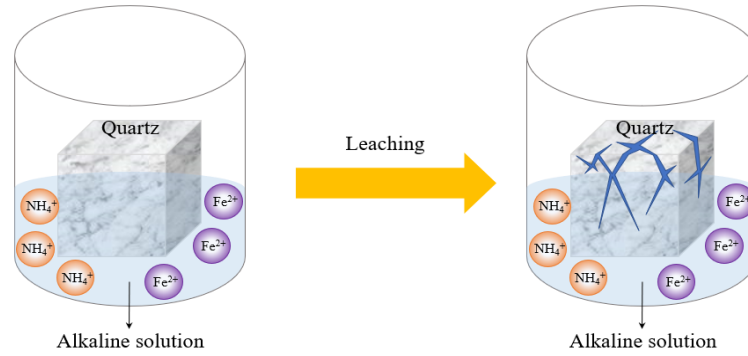


Fig. 1. Schematic diagram of quartz dissolution reaction model

Experiments on the amount of counterion are carried out for the  $\text{NH}_4^+$ -NaOH system and  $\text{Fe}^{2+}$ -NaOH system respectively. The specific experimental process is as follows: weigh 3 g of +0.045 mm-0.074 mm sample and place it in a 500 mL PTFE beaker. Then, according to the NaOH concentration of 3 mol/L, the counter ion concentration gradient is (0.01 mol/L-0.06 mol/L) to configure 300 mL solution and put them into 6 PTFE beakers. The experiment was carried out at room temperature for 6 hours, and 5 mL of supernatant was taken every 1 h for analysis.

### 2.3. Test method

#### 2.3.1. Determination of silicate ion content

The concentration of silicate ions in the leaching solution is determined by industry-standard SL 91.1-1994 silicon molybdenum yellow spectrophotometry. Soluble silicic acid reacts with ammonium molybdate in an acidic solution to form soluble yellow silicon molybdenum heteropoly acid  $[\text{H}_4\text{Si}(\text{Mo}_3\text{O}_{10})_4]$ . Within a certain concentration range, its absorbance is directly proportional to the content of soluble silicic acid. The relationship between silicate ion concentration and absorbance is  $A=0.0251+0.0930c$ ,  $R^2=0.9991$ , as shown in Fig. 2.

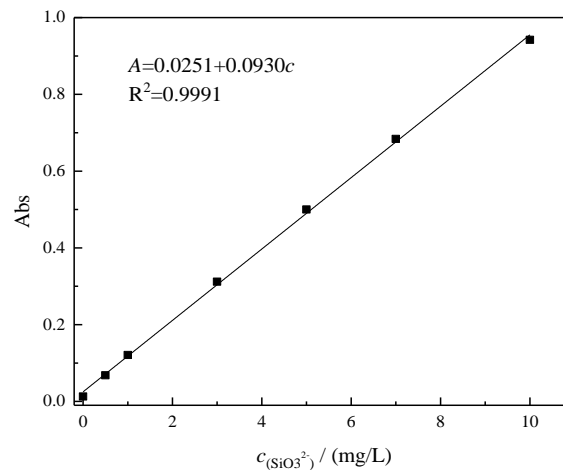


Fig. 2. Relationship between silicate ion concentration and absorbance

### 2.3.2. SEM-EDS analysis

The apparent morphology and composition of alkali dissolved quartz were analyzed by Carl Zeiss of Germany SIGMA scanning electron microscope and electron scattering spectrometer. The sample after raw ore pre-treatment is evenly scattered on the carrier sheet, and then gold-plated is placed on the scanning electron microscope carrier stage. By adjusting its multiple, the morphology of the sample is observed, and the micromorphology image acquisition and composition analysis are carried out for the required parts.

### 2.3.3. Quantum chemical calculation

Using Gaussian 16 package, geometric optimization is carried out at the theoretical level of SMD-B3LYP(D3BJ) (De Almeida et al., 2017; Allen et al., 2017) /6-311g (d, p) (Chibowski et al., 2020; A. Ali et al., 2017), and frequency analysis is carried out at the same level to verify the minimum point or transition state. Among them, to find the transition state in the reaction process, the single point energy was calculated at the SMD-B3LYP(D3BJ)/6-311g (d, p) level by using the TS (Requests optimization to a transition state rate than a local minimum, using the Berny algorithm) method (Jackson et al., 2021) with the same base level, and then the dissolution free energy of quartz was analyzed.

## 3. Results and discussion

### 3.1. Effect of counterion on alkali dissolved quartz

According to the experimental method, the experimental results are shown in Fig. 3(a). Experiments on the amount of counterion are carried out for the  $\text{NH}_4^+$ -NaOH system and  $\text{Fe}^{2+}$ -NaOH system respectively. The experimental results are shown in Fig. 3(b) and 3(c) respectively.

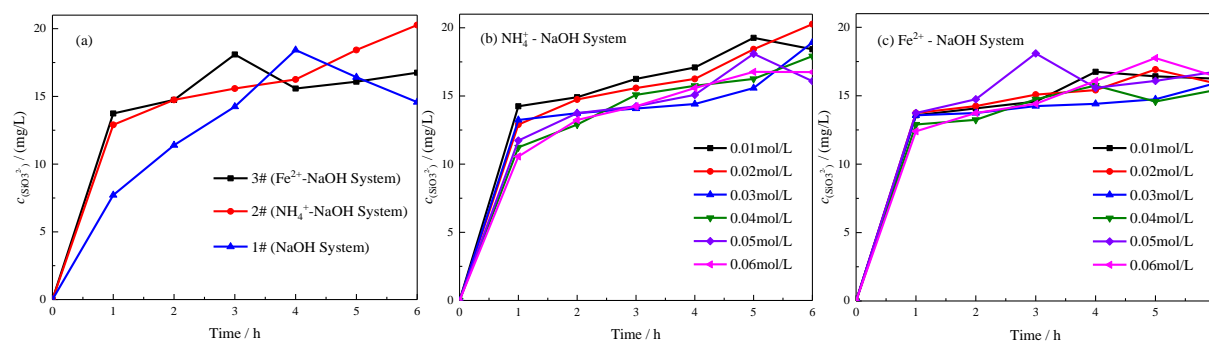


Fig. 3. Effect of counterion on alkali dissolved quartz

When the dissolution time is 6 hours, it can be seen from Fig. 3(a) that the concentration of silicate ions in the 2# system is higher than in 1# and 3#, and the concentration of silicate ions in the 3# system is significantly higher than in the 1# system. According to Fig. 3(b), when the concentration of  $\text{NH}_4^+$  is 0.02 mol/L, the concentration of silicate ion in the solution gradually increases from 1 h to 6 h, up to 20.26 mg / L. without  $\text{NH}_4^+$ , when the concentration of NaOH is 3 mol/L, the concentration of silicate ion in the solution will first increase and then decrease, and only 14.57 mg/L at 6 h. Therefore, the appropriate ammonium ion concentration will make the final dissolution effect in the system better than that in the system using NaOH. Fig. 3(c) shows that when  $\text{Fe}^{2+}$  concentration is 0.05 mg/L, the concentration of silicate ion in the solution can reach 18.09 mg/L at 3 h, which is better than 14.57 mg/L only when NaOH concentration is 3 mg/L and dissolved for 6 h. However, the reaction time needs to be strictly controlled. When the time is prolonged, the effect becomes worse, Therefore, the appropriate ion concentration and dissolution time will make the dissolution effect of this system better than that of the system using NaOH.

Our team (Tang et al., 2017; Yang et al., 2017) has conducted corresponding experiments on the alkaline leaching of Carlin type gold ores. The experimental results show that the leaching rate of gold can be improved through alkali leaching. Which indicates that alkali leaching can dissolve quartz and expose the coated gold.

The slag of pure quartz mineral dissolved in 3 mg/L NaOH solution for 6 h and the slag of pure quartz mineral dissolved in 3 mg/L NaOH solution added with  $(\text{NH}_4)_2\text{SO}_4$  and  $\text{FeSO}_4$  for 6 h were detected in SEM. The experimental results are shown in Fig. 4. It can be seen from Fig. 4 that the dissolution of quartz by NaOH makes its surface lose and porous. The dissolution of 3 mg/L NaOH for 6 h (Fig. 4(b)) shows that the addition of NaOH dissolution is conducive to the subsequent opening of quartz's wrapping of gold, and the dissolution of 0.05 mg/L  $\text{Fe}^{2+}$ -3 mg/L NaOH for 6 h (Fig. 4(d)) shows that the system is conducive to the infiltration of gold leaching agent into quartz and reaction with gold, The dissolution of 0.02 mg/L  $\text{NH}_4^+$ -3 mg/L NaOH for 6 h (Fig. 4(c)) shows that the system not only helps to open the wrapping of gold by quartz but also helps the gold leaching agent penetrate quartz and react with gold.

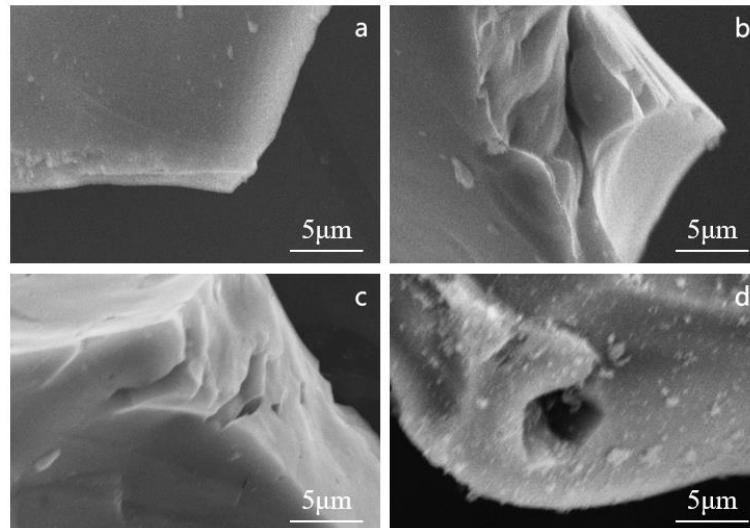


Fig. 4. SEM diagram of quartz dissolved by counterion pair NaOH: a. Raw ore; b. Slag dissolved in 3 mol/L NaOH for 6 h; c. Slag dissolved in 0.02 mol/L  $\text{NH}_4^+$ -3 mol/L NaOH for 6 h; d. Slag dissolved in 0.05 mol/L  $\text{Fe}^{2+}$ -3 mol/L NaOH for 6 h;

According to the scanning electron microscope of minerals in Fig. 4 at 5000 times, compare 4(b), 4(c), and 4(d) with 4(a) respectively. The results show that leaching makes the quartz surface loose and porous. Fig.4b shows that adding NaOH leaching is conducive to the subsequent opening of quartz's wrapping of gold. Fig. 4(d) shows that under the  $\text{Fe}^{2+}$ -NaOH system, the leaching agent will penetrate quartz and react with gold, The Fig. 4(c) diagram shows that under the  $\text{NH}_4^+$ -NaOH system, it is not only helpful to open the package of gold by quartz, but also helpful for the leaching agent to penetrate quartz and react with gold.

Energy spectrum analysis was conducted for the dissolved slag in the two systems after the introduction of the counterion, and the material composition in the dissolved slag was detected. The results are shown in Fig. 5 and Fig. 6 respectively. It can be seen from Fig. 5 that the mineral element composition in the slag dissolved by introducing counterion  $\text{NH}_4^+$  is only Si and O, and the dissolved slag is still  $\text{SiO}_2$ , while the mineral element composition in the slag dissolved by introducing counterion  $\text{Fe}^{2+}$  contains Fe in addition to Si and O (see Fig. 6), indicating that the dissolved slag contains iron oxide or iron hydroxide in addition to  $\text{SiO}_2$ .

The laser particle size analysis is carried out on the dissolved slag of quartz in the dissolution experiment of the ion  $\text{Fe}^{2+}/\text{NH}_4^+$ -NaOH system. The experimental results are shown in Fig. 7. It can be seen from Fig. 7 that the initial particle size of raw ore is +0.030  $\mu\text{m}$ -0.110  $\mu\text{m}$  range. After dissolution in the NaOH system, the particle size range becomes wider, about +0.030  $\mu\text{m}$ -0.200  $\mu\text{m}$  range, but after dissolution in the  $\text{NH}_4^+$ -NaOH system, the change of particle size range is small, and the proportion of fine particle size increases, especially at +0.040  $\mu\text{m}$ -0.070  $\mu\text{m}$  range, after dissolution in  $\text{Fe}^{2+}$ -NaOH system, the particle size range changes slightly (+0.030  $\mu\text{m}$ -0.150  $\mu\text{m}$ ), the particle size of dissolved leaching residue is mainly concentrated at 0.070  $\mu\text{m}$  nearby. When  $\text{Fe}^{2+}$  and  $\text{NH}_4^+$  are added, the particle size range of slag after dissolving quartz with NaOH is wider than that of raw ore. this is because the

hydrophobicity of quartz surface changes with the increase of leaching time, resulting in agglomeration. The agglomeration effect after adding  $\text{NH}_4^+$  is weaker than in other conditions. Therefore,  $\text{NH}_4^+$  contained in alkali wet pre-treatment has a certain "protective" effect on the surface properties of quartz dissolution, which is conducive to the exposure of exposed gold.

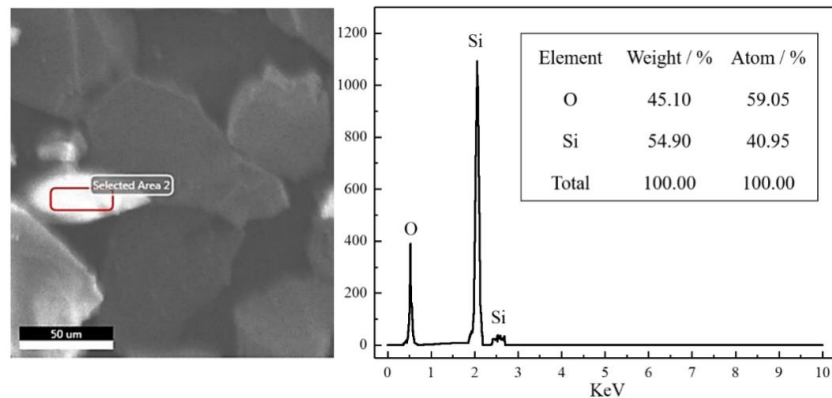


Fig. 5. EDS diagram of quartz slag dissolved in  $\text{NH}_4^+$ -NaOH system

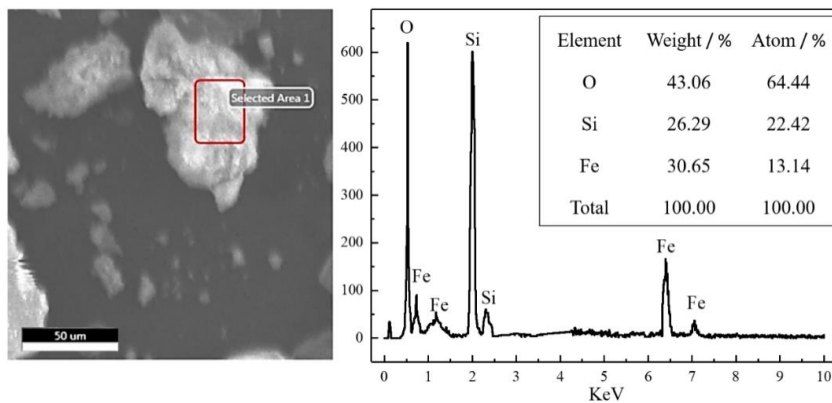


Fig. 6. EDS diagram of quartz slag dissolved in  $\text{Fe}^{2+}$ -NaOH system

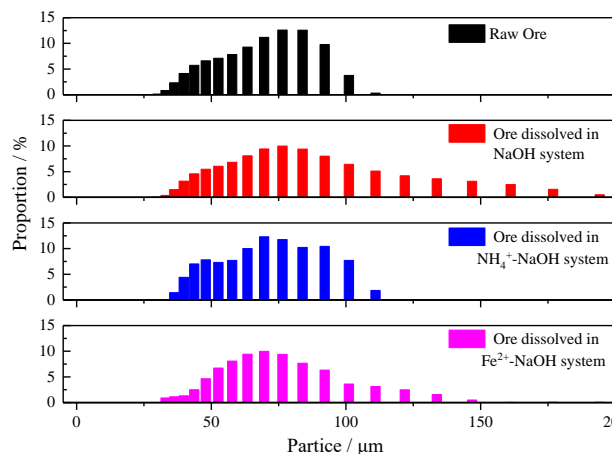


Fig. 7. Particle size analysis of slag after dissolving quartz in counterion - NaOH system

## 3.2. Dissolution mechanism

### 3.2.1. Kinetic study on alkali dissolution of quartz by counterion

By studying the leaching kinetics of quartz in the  $(\text{NH}_4)_2\text{SO}_4$ -NaOH system, the rate control steps of the dissolution process can be defined, to change the test conditions and improve the reaction rate of the dissolution process. The existing dissolution models can be classified into the particle shrinkage core

model, particle disintegration model, mixing model, and porous diffusion model. The particle shrinkage core model can be used to describe most ore dissolution processes (Z. Zhang et al., 2017). Therefore, the shrinkage core model is used for calculation in this paper.

Assuming that the quartz particles reacted in the  $(\text{NH}_4)_2\text{SO}_4\text{-NaOH}$  system are approximately spherical geometry and the dissolution process is controlled by diffusion, the dissolution kinetic equation of the shrinking core model is:

$$1 - \frac{2}{3}\alpha - (1 - \alpha)^{\frac{2}{3}} = k_1 t \quad (1)$$

If the dissolution process is controlled by chemical reaction, the dissolution kinetic equation of the shrinking core model is:

$$1 - (1 - \alpha)^{\frac{1}{3}} = k_2 \quad (2)$$

If the dissolution process is controlled by mixing (i.e., diffusion control and chemical reaction control act simultaneously), the dissolution kinetic equation affected by the shrinking core model (Abdel-Aal, 2000) can be expressed as:

$$1 - 2(1 - \alpha)^{\frac{1}{3}} + (1 - \alpha)^{\frac{2}{3}} = k_3 t \quad (3)$$

where  $\alpha$  - Ion dissolution concentration, mg/L; T - Reaction time, h;  $k_1$  - Diffusion controlled reaction rate constants;  $k_2$  - Chemical controlled reaction rate constants;  $k_3$  - Mixing controlled reaction rate constants

Dissolution temperature is an important factor affecting the DCRQ. Generally, the relationship between dissolution rate and temperature meets the Arrhenius equation (Ashraf et al., 2005):

$$k = A \cdot \exp \left[ -\frac{E_a}{RT} \right] \quad (4)$$

where k - DCRQ; A - Frequency coefficient, mol/(m<sup>2</sup>·S);  $E_a$  - Reaction activation energy, J/mol; T - Thermodynamic temperature, K; R - Gas constant, 8.314 J/(mol·K).

Formula (4) shows that the dissolution rate increases with the increase in temperature because the increase in solution temperature can accelerate the diffusion operation of molecules, enhance the activity of reagent molecules and mineral molecules, increase the collision probability, and increase the dissolution rate. According to the experimental results of the effect of early temperature on quartz dissolution,  $1-(1-\alpha)^{1/3}$  plot the time t, and the results are shown in Fig. 8. The linear regression equation, apparent rate constant and correlation coefficient ( $R^2$ ) at different dissolution temperatures are shown in table 2. According to the variant of the Arrhenius equation  $k = \ln(A) - E_a/RT$ , the Arrhenius linear diagram can be obtained by plotting the natural logarithm of the apparent rate constant of dissolution reaction at each temperature and the reciprocal 1/T of temperature in Fig. 8, as shown in Fig. 9.

It can be seen from Fig. 8 and table 2 that the dissolution kinetics of quartz in  $(\text{NH}_4)_2\text{SO}_4 - \text{NaOH}$  system under different temperature conditions can also be explained by the chemical reaction control model in the shrinking core model. The dissolution rate is greatly affected by temperature and increases significantly with the increase in temperature. The matching degree between the experimental data and the shrinking core model under the condition of temperature is not as good as that under the condition of particle size. This may be because the change in temperature changes the reaction rate and the concentration of each component in the solution, which affects the DCRQ.

Table 2. Linear regression equation, apparent rate constant, and correlation coefficient values at different dissolution temperatures ( $R^2$ )

Temperature (°C)	Chemical reaction control $1 - (1 - a)^{1/3}$		
	Linear regression equation	Apparent rate(min <sup>-1</sup> )	Correlation coefficient value ( $R^2$ )
25	y = 0.0089x + 0.0146	0.0113	0.8437
35	y = 0.0105x + 0.0107	0.0123	0.8589
45	y = 0.0128x + 0.0073	0.0140	0.8941
55	y = 0.0169x + 0.0008	0.0170	0.8818
65	y = 0.02x - 0.0012	0.0198	0.9185
75	y = 0.0228x - 0.0064	0.0217	0.9247

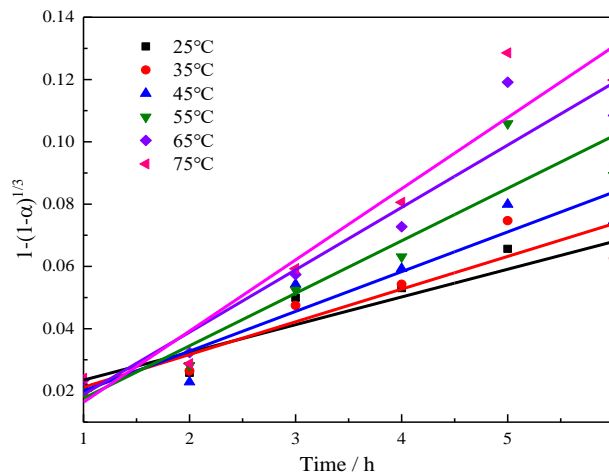


Fig. 8. Dissolution of quartz at different temperatures  $1-(1-\alpha)^{1/3}$  relation curve with experiment

It can be seen from Fig. 8 and table 2 that the dissolution kinetics of quartz in  $(\text{NH}_4)_2\text{SO}_4\text{-NaOH}$  system at different temperatures can be explained by the chemical reaction control model in the shrinking core model. The obtained data graph is approximately a straight line, indicating that DCRQ is a constant at any determined temperature, that is, DCRQ is only a function of temperature. It is consistent with the principle that DCRQ is a constant at a certain temperature, and  $E_a = 12.02$  kJ/mol can be obtained from Fig. 9. When the reaction is controlled by diffusion, the apparent activation energy is in the range of 8 kJ/mol-20 kJ/mol; When the reaction is controlled by chemical reaction, the apparent activation energy is in the range of 40 kJ/mol-300 kJ/mol (Walsh et al., 2000; A. M. Ali et al., 2020). According to this principle, the dissolution kinetic model of quartz in the  $(\text{NH}_4)_2\text{SO}_4\text{-NaOH}$  system should belong to the diffusion control in the shrinking core model.

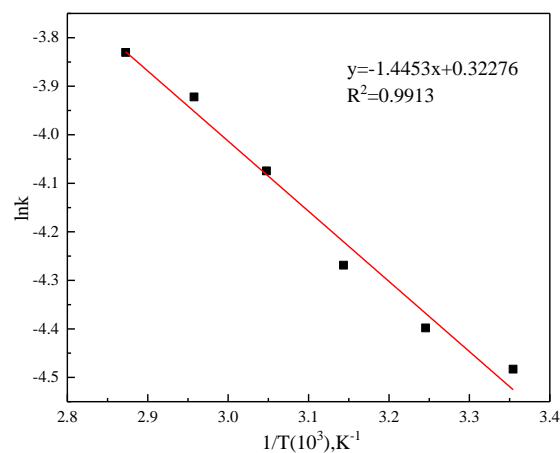


Fig. 9. Arrhenius diagram of quartz dissolution in  $\text{NH}_4^+\text{-NaOH}$  system

### 3.2.2. Quantum chemical calculation of alkali dissolved quartz by counterion

Advanced ab initio calculation (Q. Cao et al., 2023) is very successful in predicting mineral structure and physical properties. The most important thing is that the whole structure and energy of minerals can be expressed by small molecular clusters, small-scale directional forces, or covalent bonds. Therefore, using limited molecular clusters can simulate the local structure of the mineral surface and provide a deeper bond analysis between mineral atoms. The mechanism and process of the quartz solution interface reaction can be described more clearly by using quantum chemistry to study the related transition compounds in the dissolution reaction on the surface of the quartz.

All reactions in this paper are simulated by using the Gaussian 16 program package and density functional theory (DFT) method in the ab initio method. DFT method (Y. Zhang et al., 2007) considers electronic correlation, which has more advantages in dealing with weak bonds (free energy, etc.), and

is better in accuracy than the Hartree Fock method without considering electronic correlation (S. Zhang & Liu, 2014). In addition, DFT is more rapid and effective in dealing with large molecular cluster systems. Therefore, the DFT method is used to compare the free energy of NaOH,  $\text{NH}_4^+$ -NaOH, and  $\text{Fe}^{2+}$ -NaOH systems. So far, the calculation research on the reaction mechanism of the quartz water interface has mainly focused on B3LYP (Shinohara & Tsubouchi, 2020) and M05 (Linder & Rodgers, 2015). Because B3LYP is not very accurate in calculating the intermolecular reaction and dealing with the interaction between weak bonds, M05 has a large error in calculating the transition metal elements, and the solution free energy of the studied system needs to be considered. In addition, the accuracy of the calculation results is very important in a class of studies involving the calculation of system energy, free energy, and dissolution free energy using the traditional transition state theory. At present, the 6-31+G\*\* base level is widely used in the study of mineral dissolution (J. Y. Zhang et al., 2020), but to obtain higher accuracy, many scholars use the higher base level 6-311+G\*\* (Tamang et al., 2022) all electronic calculation method. To find the reaction transition state, the methods available are TS, STQN, NEB, and GSM, among which the TS method is highly recognized in the process of use (Jackson et al., 2021).

Based on comprehensive consideration, geometric optimization is carried out at the theoretical level of SMD-B3LYP(D3BJ) (De Almeida et al., 2017; Allen et al., 2017) / 6-311 g(d, p) (Chibowski et al., 2020; A. Ali et al., 2017), and frequency analysis is carried out at the same level to verify the minimum point or transition state, in which the transition state in the reaction process is found, and TS (Requests optimization to a transition state rather than a local minimum) of the same base level is adopted. Using the Beryny algorithm, the single point energy is calculated at the SMD-B3LYP(D3BJ) / 6-311+G\*\* level, and then the dissolution-free energy of quartz is analyzed.

#### • NaOH system

The calculation results of the dissolution reaction path and stable point configuration of quartz in the NaOH system are shown in Fig. 10. For the convenience of analysis, the bond length and bond angle are arranged in table 3.

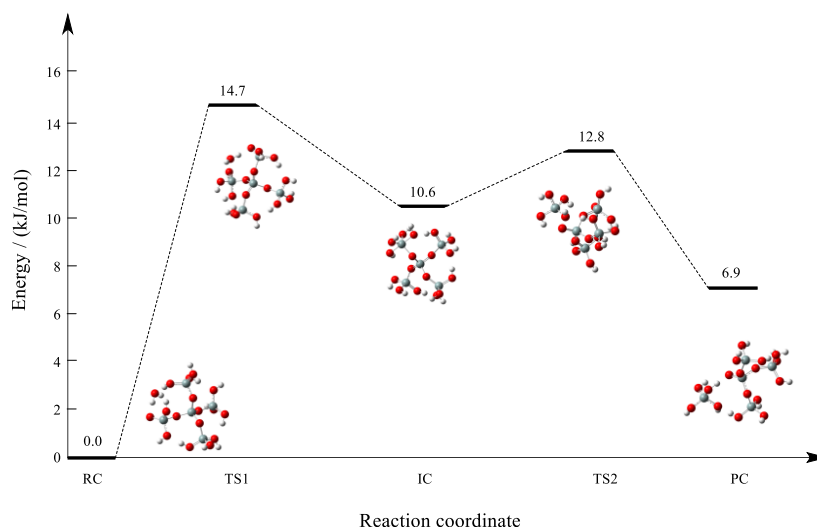


Fig. 10. Reaction path of quartz dissolution in NaOH system

It can be seen from the potential energy profile that the generation of an intermediate (IC) product in the dissolution process means that there are two transition states (TS1 and TS2). In the whole reaction path, the energy barrier height of the first transition state (TS1) is higher than that of the second transition state (TS2). It is inferred that the first transition state (TS1) is the key to restricting the DCRQ

The acidic hydroxyl groups at the interface between quartz and solvent are neutralized and deprotonated by alkaline substances and form stable compounds through hydrogen bonding with a solvent water molecule. Then the negatively charged silicon-oxygen species undergo double electron transfer to the water molecule to capture the protons of the water molecule. At the same time, the negative charge density increases, and the oxygen atoms in the water molecule undergo nucleophilic

addition to another silicon center, the free energy of this process is 14.7 kJ/mol. This process leads to the emergence of five coordinated silicon intermediates. At this time, the hybridization mode of silicon atoms attacked by nucleophiles changes from  $sp^3$  to  $sp^3d$ , that is, due to the participation of the d orbital, silicon can form a relatively stable five-coordinated intermediate, and its free energy is 10.6 kJ/mol higher than that of the starting compound. Due to the high charge density of silicon central five coordination, another Si-O bond can be eliminated and separated in the form of a silicate. This elementary process is an elimination process, and the free energy of the reaction is 12.8 kJ/mol. As the result, it is manifested as the dissolution of the contact interface between quartz and solvent, and the whole body is manifested as a nucleophilic addition elimination reaction, and the free energy is finally reduced to 6.9 kJ/mol.

In the NaOH system, the bond length of reactant (RC)  $Si_9-O_{w27}$  is optimized to be 3.3376 Å. In the reaction process, it becomes 2.6184 Å in the first transition state (TS1), decreases to 1.7428 Å in the intermediate product (IC), becomes 1.6488 Å in the second transition state (TS2), and shortens to 1.6152 Å in the last product (PC), that is, O in  $H_2O$  finally forms a bond with Si in  $SiO_2$ , A new product  $Si(OH)_4$  was formed, the reaction model diagram is shown in Fig. 11.

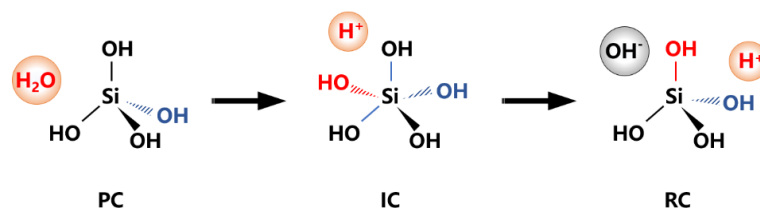


Fig. 11. Quartz dissolution reaction model in NaOH system

In the NaOH system, the change of bond angle of four O atoms connected with  $Si_1$  was focused. It was found that  $Si_9-O_3-Si_1$  increased first, then decreased, and finally increased slightly in the reaction process from reactant (RC) to product (PC);  $Si_5-O_4-Si_1$  increased first, then decreased, and finally increased; The bond angle of  $Si_7-O_2-Si_1$  in the first transition state (TS1) and intermediate (IC) increased to  $137.6828^\circ$  and  $143.4896^\circ$  respectively, decreased to  $141.5876^\circ$  in the second transition state, but increased to  $149.5525^\circ$  in the product (PC);  $Si_8-O_5-Si_1$  shows a fluctuating state of first increasing and then decreasing, and then increasing and decreasing. The bond angle in the final product (PC) is  $131.9595^\circ$ . This series of changes shows that the dissolution process of quartz in the NaOH system is a complex dynamic change, which is difficult to quantify. Reaction equation:  $-O(OH)_2Si-O-Si(OSi(OH)_3)_3 + H_2O \rightarrow (OH)_3Si-OH + -O-Si(OSi(OH)_3)_3$ .

#### • $NH_4^+$ - NaOH system

The calculation results of the path and stable point configuration of quartz dissolution reaction in the  $NH_4^+$ - NaOH system are shown in Fig. 12. It can be seen from the potential energy profile that an intermediate (IC) product is also produced in the dissolution process, which means that there are two transition states (TS1 and TS2) in the whole reaction path, and the energy barrier height of the first transition state (TS1) is higher than that of the second transition state (TS2). Therefore, it can be inferred that the first transition state (TS1) is the key to the rate of quartz dissolution.

The acidic hydroxyl group on the interface side of quartz in contact with the solvent is neutralized and deprotonated by alkaline substances, and forms a stable compound with a solvent water molecule through a hydrogen bond. Then, the negatively charged silicon-oxygen species undergo double electron transfer to the water molecule to capture the proton of the water molecule. At the same time, with the increase of negative charge density, the oxygen atom in the water molecule has a nucleophilic addition process to another silicon center, and the free energy of this process is 10.1 kJ/mol. This process leads to the emergence of five coordinated silicon intermediates. At this time, the hybridization mode of silicon atoms attacked by nucleophiles changes from  $sp^3$  to  $sp^3d$ , that is, due to the participation of the d orbital, silicon can form a relatively stable five coordinated intermediate, and its free energy is 8.6 kJ/mol higher than that of the starting compound. Due to the high charge density of silicon central five coordination, another Si-O bond can be eliminated and separated in the form of a silicate. This elementary process is an elimination process, and the free energy of the reaction is 9.4 kJ/mol. the result

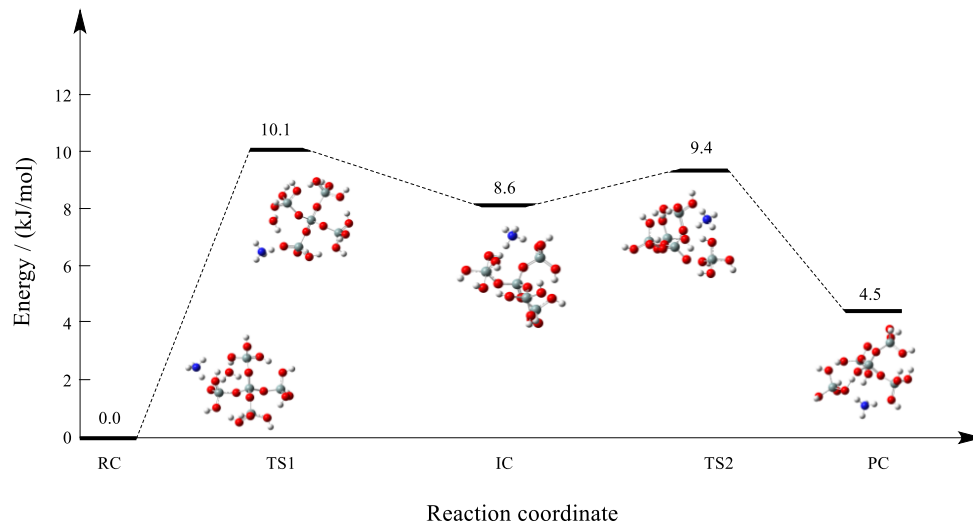


Fig. 12. Reaction path of quartz dissolution in  $\text{NH}_4^+$ -NaOH system

is the dissolution of the contact interface between quartz and solvent. In the  $\text{NH}_4^+$ -NaOH system, the dissolution of quartz is a nucleophilic addition elimination reaction, and the free energy is finally reduced to 4.5 kJ/mol. Compared with the NaOH system, the introduction of  $\text{NH}_4^+$  can promote the dissolution of quartz. During the reaction process of quartz dissolution,  $\text{NH}_4^+$  does not break the chemical bond and change the valence state but forms a double electric layer structure as the counter ion and the hydroxylated surface of the quartz. It affects the concentration and dispersion of quartz particles through electrostatic action, increases the specific surface area of quartz, and then promotes the dissolution of quartz.

In the  $\text{NH}_4^+$ -NaOH system, the bond length of reactant (RC)  $\text{Si}_8\text{-O}_{w27}$  is optimized to be 3.4336 Å. During the reaction, it becomes 2.5578 Å in the first transition state (TS1), 1.7421 Å in the intermediate product (IC), 1.6588 Å in the second transition state (TS2), and 1.5958 Å in the final product (PC). That is, O in  $\text{H}_2\text{O}$  finally forms a bond with Si in  $\text{SiO}_2$  to form a new product  $\text{Si}(\text{OH})_4$ , the reaction model diagram is shown in Fig. 13.

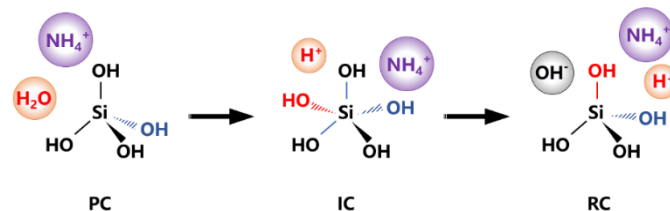


Fig. 13. Quartz dissolution reaction model in  $\text{NH}_4^+$ -NaOH system

In the  $\text{NH}_4^+$ -NaOH system, the change of bond angle of four O atoms connected to  $\text{Si}_1$  is focused. In the process from reactant (RC) to product (PC),  $\text{Si}_9\text{-O}_3\text{-Si}_1$  first increases and then decreases, from the initial  $133.3613^\circ$  to  $102.9063^\circ$ ,  $\text{Si}_5\text{-O}_4\text{-Si}_1$  first increases and then decreases, and finally increases.  $\text{Si}_7\text{-O}_2\text{-Si}_1$  is in the first transition state (TS1) In the intermediate (IC) and the second transition state (TS2), the bond angle increases to  $138.4767^\circ$ ,  $139.7920^\circ$ , and  $145.9772^\circ$  respectively, but decreases to  $136.6560^\circ$  in the product (PC), and the bond angle of  $\text{Si}_8\text{-O}_5\text{-Si}_1$  increases gradually, and the bond angle in the final product (PC) can reach  $141.5376^\circ$ . This change shows that the dissolution process of quartz in  $\text{NH}_4^+$ -NaOH system also belongs to complex dynamic change, which is difficult to quantify. Reaction equation:  $-\text{O}(\text{OH})_2\text{Si}-\text{O}-\text{Si}(\text{OSi}(\text{OH})_3)_3 + \text{NH}_3 \cdot \text{H}_2\text{O} \rightarrow (\text{OH})_3\text{Si}-\text{OH} + -\text{O}-\text{Si}(\text{OSi}(\text{OH})_3)_3 + \text{NH}_4^+$ .

#### • $\text{Fe}^{2+}$ -NaOH system

The calculation results of the quartz dissolution reaction path and stable point configuration in the  $\text{Fe}^{2+}$ -NaOH system are shown in Fig. 14. It can be seen from the potential energy profile that intermediate (IC) products will be produced in the dissolution process, which means that there are two transition states (TS1 and TS2) in the whole reaction path, and the energy barrier height of the first transition state

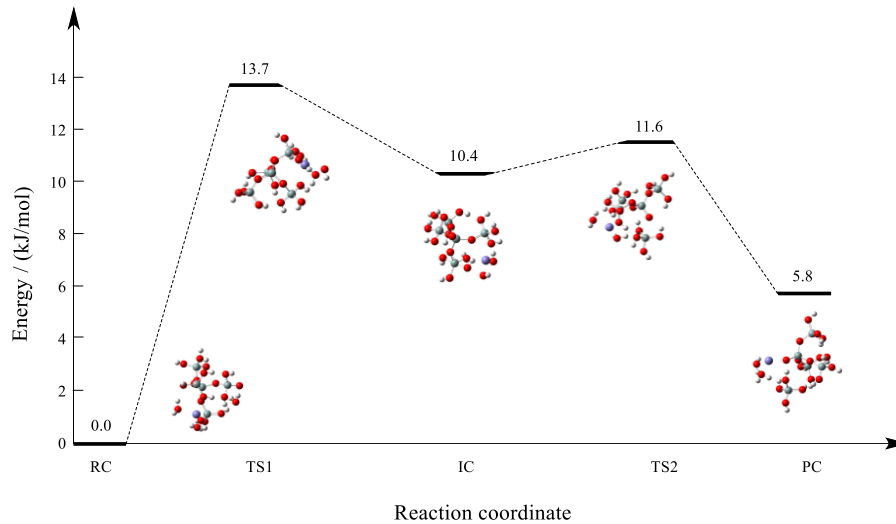


Fig. 14. Reaction path of quartz dissolution in  $\text{Fe}^{2+}$ -NaOH system

(TS1) is higher than that of the second transition state (TS2). Therefore, it is inferred that the first transition state (TS1) is the key to restricting the DCRQ.

The acidic hydroxyl group on the interface side of quartz in contact with the solvent is neutralized and deprotonated by alkaline substances, and forms a stable compound with a solvent water molecule through a hydrogen bond. Then, the negatively charged silicon-oxygen species undergo double electron transfer to the water molecule to capture the proton of the water molecule. At the same time, the negative charge density increases, and the oxygen atom in the water molecule has a nucleophilic addition process to another silicon center. The free energy of this process is 13.7 kJ/mol. This process leads to the emergence of five coordinated silicon intermediates. At this time, the hybridization mode of silicon atoms attacked by nucleophiles changes from  $\text{sp}^3$  to  $\text{sp}^3\text{d}$ , that is, due to the participation of the d orbital, silicon can form a relatively stable five-coordinated intermediate, and its free energy is 10.4 kJ/mol higher than that of the starting compound. Due to the high charge density of the five coordination in the silicon center, another Si-O bond can be eliminated and separated in the form of a silicate. This elementary process is an elimination process, and the free energy of the reaction is 11.6 kJ/mol. As the result, it is manifested as the dissolution of the contact interface between quartz and solvent, and as a whole, it is a nucleophilic addition elimination reaction, and the free energy is finally reduced to 5.8 kJ/mol. Compared with the NaOH system, the introduction of  $\text{Fe}^{2+}$  can also promote the dissolution of quartz, but its promotion effect is slightly worse than  $\text{NH}_4^+$ . During the reaction process of quartz dissolution,  $\text{Fe}^{2+}$  does not participate in the reaction but acts as counter ions like  $\text{NH}_4^+$ , forming a double electric layer. It affects the concentration and dispersion of quartz particles through electrostatic action, increases the specific surface area of quartz, and then promotes the dissolution of quartz.

In the  $\text{Fe}^{2+}$ -NaOH system, the bond length of reactant (RC)  $\text{Si}_8\text{-O}_{w27}$  is optimized to be 3.3800 Å. During the reaction, it becomes 3.5710 Å in the first transition state (TS1), 1.8446 Å in the intermediate product (IC), 1.6615 Å in the second transition state (TS2), and 1.6453 Å in the final product (PC), that is, O in  $\text{H}_2\text{O}$  finally forms a bond with Si in  $\text{SiO}_2$ , A new product  $\text{Si}(\text{OH})_4$  was formed, the reaction model diagram is shown in Fig. 15.

In the  $\text{Fe}^{2+}$ -NaOH system, we still focus on the change of the bond angle of the four O atoms connec-

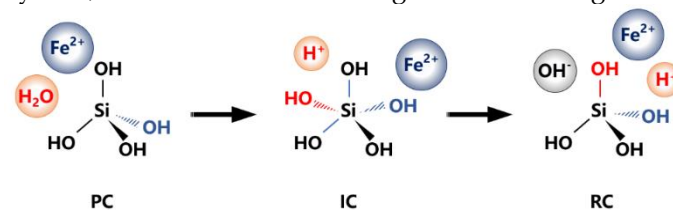


Fig. 15. Quartz dissolution reaction model in  $\text{Fe}^{2+}$ -NaOH system

ted to Si<sub>1</sub>. It can be found that in the process from reactant (RC) to product (PC), Si<sub>8</sub>-O<sub>3</sub>-Si<sub>1</sub> gradually decreases from the initial 144.7869° to 105.863°, Si<sub>36</sub>-O<sub>4</sub>-Si<sub>1</sub> first decreases and then increases, and the bond angle of Si<sub>6</sub>-O<sub>2</sub>-Si<sub>1</sub> in the first transition state (TS1) increases to 152.7539°, The intermediate (IC) decreased to 142.6560° and 129.1960° respectively in the second transition state (TS2), but increased to 168.0335° in the product (PC). The bond angle of Si<sub>7</sub>-O<sub>5</sub>-Si<sub>1</sub> always decreased first, then increased, and finally decreased. The bond angle in the final product (PC) decreased to 128.3953°. This change shows that in the Fe<sup>2+</sup>-NaOH system, the dissolution process of quartz is also a complex dynamic change, which is difficult to quantify. Reaction equation:



In NaOH, NH<sub>4</sub><sup>+</sup>-NaOH, and Fe<sup>2+</sup>-NaOH systems, the comparison of bond length and bond angle in the quartz dissolution path "Reactant-First transition state-Intermediate-Second transition state-Product" is shown in table 3. In the three systems, the bond length of quartz dissolved in the whole reaction path decreases, and the change of bond angle has no obvious law.

Table 3. Bond length and bond angle in quartz dissolution reaction path in three systems

Reaction path	NaOH system		NH <sub>4</sub> <sup>+</sup> -NaOH system		Fe <sup>2+</sup> -NaOH system	
	Bond length (Å)	Bond angle (°)	Bond length (Å)	Bond angle (°)	Bond length (Å)	Bond angle (°)
RC	3.3376	134.4139	3.4336	133.3613	3.3800	144.7869
TS1	2.6184	137.5121	2.5578	140.0701	3.5710	140.9905
IC	1.7428	133.7785	1.7421	132.6722	1.8446	135.4075
TS2	1.6488	128.4858	1.6588	131.0259	1.6615	130.0119
PC	1.6152	130.4302	1.5958	102.9063	1.6453	105.8631

#### 4. Conclusions

- (1) In the Fe<sup>2+</sup>-NaOH system, when the Fe<sup>2+</sup> concentration is 0.05 mol/L, the concentration of silicate ions in the solution can reach 18.09 mg/L after quartz is dissolved for 3 h which is better than the effect in the NaOH system. As a counterion like NH<sub>4</sub><sup>+</sup>, Fe<sup>2+</sup> aggregation, retention, and release in the alkaline solution, forming a double electric layer structure with the hydroxylated quartz surface through electrostatic interaction, and then control the dispersion degree of particles to increase the specific surface area of quartz. The results of SEM-EDS and laser particle size analysis are consistent with the experimental results.
- (2) In the (NH<sub>4</sub>)<sub>2</sub>SO<sub>4</sub>-NaOH system, the influence of quartz dissolution temperature on the dissolution of quartz conforms to the chemically controlled shrinking nucleus kinetic equation  $1-(1-\alpha)^{1/3} = kt$ , the apparent free energy is 12.02 kJ/mol, within the range of diffusion control, which shows that NaOH dissolved quartz has the particularity of meeting both chemical control and diffusion control under the influence of counterion.
- (3) Calculate the Si-O<sub>w</sub> bond length and Si-O<sub>3</sub>-Si bond angle in the three dissolved quartz systems of NaOH, NH<sub>4</sub><sup>+</sup>-NaOH, and Fe<sup>2+</sup>-NaOH, the quartz is dissolved in the "Reactant-First transition state-Intermediate-Second transition state-Product". The bond length of the reaction path decreases in the entire reaction path, but there is no obvious law of bond angle changes. In the three dissolved quartz systems, the reactions belong to a nucleophilic addition-elimination, which will form new products-Si(OH)<sub>4</sub>. The three reaction equations are:
  - $-\text{O}(\text{OH})_2\text{Si}-\text{O}-\text{Si}(\text{OSi}(\text{OH})_3)_3 + \text{H}_2\text{O} \rightarrow (\text{OH})_3\text{Si}-\text{OH} + -\text{O}-\text{Si}(\text{OSi}(\text{OH})_3)_3$ ,
  - $-\text{O}(\text{OH})_2\text{Si}-\text{O}-\text{Si}(\text{OSi}(\text{OH})_3)_3 + \text{NH}_3 \cdot \text{H}_2\text{O} \rightarrow (\text{OH})_3\text{Si}-\text{OH} + -\text{O}-\text{Si}(\text{OSi}(\text{OH})_3)_3 + \text{NH}_4^+$ ,
  - $-\text{O}(\text{OH})_2\text{Si}-\text{O}-\text{Si}(\text{OSi}(\text{OH})_3)_3 + \text{Fe}^{2+} + 3\text{H}_2\text{O} \rightarrow \text{Si}(\text{OH})_3\text{Si}-\text{OH} + -\text{O}-\text{Si}(\text{OSi}(\text{OH})_3)_3 + \text{Fe}^{2+} + 2\text{H}_2\text{O}$ .
 In addition, the primary minimum energies are 14.7 kJ/mol, 10.1 kJ/mol, and 13.7 kJ/mol.

#### Acknowledgments

This work was supported by the National Natural Science Foundation of China (51864010) and the Plan Project of Science and Technology of Guizhou Province of China (Qiankehe Foundation [2017]1404,

Qiankehe Platform Talents [2018]5781, Qiankehe JS [2011]2326 and Qiansheng Special Combination [2012]153.

## References

- ABDEL-AAL, E. A., 2000. *Kinetics of Sulfuric Acid Leaching of Low-Grade Zinc Silicate Ore*. Hydrometallurgy, 55(3): 247–254.
- ALI, A. M., YAHYA, N., MIJINYAWA, A., KWAYA, M. Y., SIKIRU, S., 2020. *Molecular simulation and microtextural characterization of quartz dissolution in sodium hydroxide*. Journal of Petroleum Exploration and Production Technology, 10(7), 2669–2684.
- ALI, A., PADMANABHAN, E., BAILOUMY, H., 2017. *Characterization of Alkali-Induced Quartz Dissolution Rates and Morphologies*. Arabian Journal for Science and Engineering, 42, 1–13.
- ALLEN, N., MACHESKY, M. L., WESOLOWSKI, D. J., KABENGI, N., 2017. *Calorimetric study of alkali and alkaline-earth cation adsorption and exchange at the quartz-solution interface*. Journal of Colloid and Interface Science, 504: 538–548.
- AL-SAEDI, H. N., BRADY, P. V., FLORI, R. E., HEIDARI, P., 2019. *Insights into the role of clays in low salinity water flooding in sand columns*. Journal of Petroleum Science and Engineering, 174, 291–305.
- ASHRAF, M., ZAFAR, Z. I., ANSARI, T. M., 2005. *Selective leaching kinetics and upgrading of low-grade calcareous phosphate rock in succinic acid*. Hydrometallurgy, 80(4), 286–292.
- BASTRZYK, A., POLOWCZYK, I., SADOWSKI, Z., SIKORA, A., 2011. *Relationship between properties of oil/water emulsion and agglomeration of carbonate minerals*. Sep. Purif. Technol. 77, 325–330.
- CAO, Q., YAN, W., LIU, D., WEN, S., LI, Y. (2023). *New insights into pyrite-hydrogen peroxide interactions during froth flotation: experimental and DFT study*. Physicochemical Problems of Mineral Processing, 59(1), 157409.
- CAO, X. W., CHEN, Q. D., HUA, F., ZHANG, L., SAULIUS, J., SUN, H. B., 2018. *Liquid-Assisted Femtosecond Laser Precision-Machining of Silica*. Nanomaterials, 8(5), 287.
- CHEN, B., DENG, J., WEI, H., JI, X., 2019. *Trace Element Geochemistry in Quartz in the Jinqingding Gold Deposit, Jiaodong Peninsula, China: Implications for the Gold Precipitation Mechanism*. Minerals, 9(5), 326.
- CHIBOWSKI, S., WIŚNIEWSKA, M., WAWRZKIEWICZ, M., HUBICKI, Z., GONCHARUK, O., 2020. *Electrokinetic properties of silica-titania mixed oxide particles dispersed in aqueous solution of C.I. Direct Yellow 142 dye – effects of surfactant and electrolyte presence*. Physicochemical Problems of Mineral Processing, 56(6), 123612
- DE ALMEIDA, C. F., DE ANDRADE, R. C., DE OLIVEIRA, G. F., SUEGAMA, P. H., DE ARRUDA, E. J., TEXEIRA, J. A., DE CARVALHO, C. T., 2017. *Study of Porosity and Surface Groups of Activated Carbons Produced from Alternative and Renewable Biomass: Buriti Petiole*. Orbital - The Electronic Journal of Chemistry, 9(1), 18–26.
- GUI, Q., WANG, S., ZHANG, L., 2021. *The mechanism of ultrasound oxidation effect on the pyrite for refractory gold ore pretreatment*. Arabian Journal of Chemistry, 14(4), 103045.
- HUNTER, N. J. R., VOISEY, C. R., TOMKINS, A. G., WILSON, C. J. L., LUZIN, V., STEPHEN, N. R., 2021. *Deformation Mechanisms in Orogenic Gold Systems During Aseismic Periods: Microstructural Evidence from the Central Victorian Gold Deposits, Southeast Australia*. Economic Geology, 116(8), 1849–1864.
- JACKSON, R., ZHANG, W., PEARSON, J., 2021. *TSNet: Predicting transition state structures with tensor field networks and transfer learning*. Chemical Science, 12(29): 10022–10040.
- JIAN, W., MAO, J., LEHMANN, B., COOK, N. J., XIE, G., LIU, P., DUAN, C., ALLES, J., NIU, Z., 2021. *Au-Ag-Te-rich melt inclusions in hydrothermal gold-quartz veins, Xiaojinling lode gold district, central China*. Economic Geology, 116(5), 1239–1248.
- LI, H., LI, Z., JIN, J., HAN, Y., LI, Y., 2022. *Pore Evolution in Refractory Gold Ore Formed by Oxidation Roasting and the Effect on the Cyanide Leaching Process*. ACS Omega. 7(4), 3618–3625.
- LINDER, D. P., RODGERS, K. R., 2015. *Methanethiol Binding Strengths and Deprotonation Energies in Zn(II)-Imidazole Complexes from M05-2X and MP2 Theories: Coordination Number and Geometry Influences Relevant to Zinc Enzymes*. The Journal of Physical Chemistry B. 119(37), 12182–12192
- LIPATIEVA, T. O., LIPATIEV, A. S., KULAKOVA, Y. V., LOTAREV, S. V., FEDOTOV, S. S., PRUSOVA, I. V., SIGAEV, V. N., 2022. *Control of Liquid Laser-Induced Etching of Quartz Glass*. Glass and Ceramics, 78(9), 345–349.
- LIU, X., LI, Q., ZHANG, Y., JIANG, T., YANG, Y., XU, B., HE, Y., 2019. *Improving gold recovery from a refractory ore via Na<sub>2</sub>SO<sub>4</sub>-assisted roasting and alkaline Na<sub>2</sub>S leaching*. Hydrometallurgy, 185, 133–141.
- MA, J., TANG, Y., YANG, D. Q., PEI, P., 2020. *Kinetics of advanced oxidative leaching of pyrite in a potassium peroxydisulphate solution*. Journal of the Southern African Institute of Mining and Metallurgy, 120(2), 165–172.

- SHINOHARA, Y., TSUBOUCHI, N., 2020. *Effect of the electronic state on low-rank coals with Ca<sup>2+</sup> ion exchange*. Journal of Molecular Structure, 1218, 128544.
- TAMADA, O., GIBBS, G. V., JR, M. B. B., RIMSTIDT, J. D., 2012. *Silica dissolution catalyzed by NaOH: Reaction kinetics and energy barriers simulated by quantum mechanical strategies*. Journal of Mineralogical and Petrological Sciences, 107(2), 87–98.
- TAMANG, S., THAPA, A., CHETTRI, K., DATTA, B., BISWAS, J., 2022. *Analysis of dipyridine dipyrrole-based molecules for solar cell application using computational approach*. Journal of Computational Electronics, 21(1), 94–105.
- TANG, Y., LI, G., YANG, Y., MA, J., ZHI, Y., YAO, Y., ZHENG, L., TUO, B., 2021. *Oxidation of Gold-Bearing Pyrite by Ammonium Persulfate*. Journal of Sustainable Metallurgy, 7(3), 1280–1292.
- TANG, Y., YANG, D., TANG, L., WANG Y., 2017. *Study on two-stage pretreatment non cyanide leaching of micro disseminated refractory gold ore*. Mining and Metallurgical Engineering, 37(1), 60–63.
- WALSH, T., WILSON, M., SUTTON, A., 2000. *Hydrolysis of the amorphous silica surface. II. Calculation of activation barriers and mechanisms*. The Journal of Chemical Physics, 113, 9191–9201.
- YANG, D., TANG, Y., TANG, L., WANG, J., WANG, H., 2017. *Study on enhanced wet pretreatment of micro disseminated gold ore*. Precious metals, 38(4), 44–48+55.
- ZHANG, J. Y., CHEN, G. L., DONG, J., WANG, P., GONG, X. D., 2020. *Design and exploration of 5-nitro-3-trinitromethyl-1H-1,2,4-triazole and its derivatives as energetic materials*. Molecular Diversity, 25(4), 2107–2121.
- ZHANG, S., HAN, G., YU, R., WEN, Z., XU, M., YANG, Y., 2021. *The Sustainable Development Path of the Gold Exploration and Mining of the Sanshan Island-Jiaojia Belt in Laizhou Bay: A DID-SVAR Approach*. Sustainability, 13(21): 11648.
- ZHANG, S., LIU, Y., 2014. *Molecular-level mechanisms of quartz dissolution under neutral and alkaline conditions in the presence of electrolytes*. Geochemical Journal, 48(2), 189–205.
- ZHANG, Y., LI, Z. H., TRUHLAR, D. G., 2007. *Computational Requirements for Simulating the Structures and Proton Activity of Siliceous Materials*. Journal of Chemical Theory and Computation, 3(2), 593–604.
- ZHANG, Z., SU, W., TANG, B., XU, W., XIONG, Z., GAO, Y., PENG, B., 2017. *Effects of isopropyl alcohol and acetic acid on surface roughness of Z - cut quartz etched by ammonium bifluoride solution*. Micro & Nano Letters, 12(10), 781 – 783.
- DRZYMALA, J., 2007. *Mineral processing. Foundations of theory and practice of minerallurgy*. Ofic. Wyd. PWr, Wroclaw, Poland.